Friction and wear behavior of WS2/Zr self-lubricating soft coatings in dry sliding against 40Cr hardened steel balls

Yunsong Lian, Jianxin Deng, Shipeng Li, Guangyuan Yan, Shuting Lei

Published Version Information

Citation: Lian, Y., Deng, J., Li, S., Yan, G., & Lei, S. (2014). Friction and wear behavior of WS2/Zr self-lubricating soft coatings in dry sliding against 40Cr-hardened steel balls. Tribology Letters, 53(1), 237-246.

Digital Object Identifier (DOI): doi:10.1007/s11249-013-0261-4

Publisher's Link: http://link.springer.com/article/10.1007/s11249-013-0261-4

Friction and wear behavior of WS_2/Zr self-lubricating soft coatings in dry sliding against 40Cr hardened steel balls

Yunsong Lian[a], Jianxin Deng[a], Shipeng Li[a], Guangyuan Yan[a], Shuting Lei[b]

[a]*School of Mechanical Engineering, Shandong University, Jinan, 250061, PR China*

[b]*Department of Industrial and Manufacturing Systems Engineering, Kansas State University, Manhattan, KS 66506, USA*

***Keywords*:** WS_2/Zr self-lubricating soft coating; Friction and wear behavior; Medium-frequency magnetron sputtering; Wear rate; Self-lubricating and wear mechanism; Dry sliding.

Abstract. WS_2 and WS_2/Zr self-lubricating soft coatings were produced by medium-frequency magnetron sputtering, multi-arc ion plating and ion beam assisted deposition technique on the cemented carbide YT15 (WC+15%TiC+6%Co) substrates. Microstructural and fundamental properties of these coatings were examined. Sliding wear tests against 40Cr hardened steel using a ball-on-disk tribometer method were carried out with these coated materials. The friction coefficient and wear rates were measured with various applied loads and sliding speeds. The wear surface features of the coatings were examined using SEM. The results showed that the WS-1 specimen (with WS_2/Zr composite coating) has higher hardness and coating/substrate critical load compared with that of the WS-2 specimen (only with WS_2 coating). The friction coefficient of WS-1 specimen increases with the increase in applied load, and is quite insensitive to the sliding speed. The wear rate of the WS-1 specimen is almost constant under different applied loads and sliding speeds. The WS-1 specimen shows the smallest friction coefficient and wear rate among all the specimens tested under the same conditions. The WS-1 specimen exhibits improved friction behavior to that of the WS-2 specimen, and the antiwear lifetime of the WS_2 coatings can be prolonged through adding Zr additives. The self-lubricating and wear mechanism of the WS_2/Zr coating was also found from the sliding wear tests.

1 Introduction

Recent advances in coatings technologies now permit the deposition of films with properties unachievable a decade ago. New coating deposition techniques developed offer a wide variety of

possibilities to tailor surfaces with many different materials and structures. In particular, chemical vapour deposition and physical vapour deposition (PVD) techniques have made it possible to deposit thin coatings a few micrometre thick in a temperature range from very high temperatures (1000℃) down to room temperature. Nowadays, coating materials such as TiN, TiC, TiCN, TiAlN, ZrN, HfN, Al_2O_3, MoS_2 and more recently WS_2 and their combinations as multilayers have been used with great success [1-4]. The first generation PVD coatings featured TiN as the hard coating and were applied in interrupted cutting. The superior performance of PVD TiN coated tools prompted their use in machining applications, such as turning, boring, as well as in industries as a wear resistant or protective layer on dies [5, 6]. The continued success of PVD coated tools led to the commercial development of the second and third generation PVD coatings (TiCN and TiAlN) which offer even higher machining productivity [7-9].

Hard coatings such as TiN, TiC, TiAlN, ZrN, and Al_2O_3 and their combinations as multilayers have been widely used to increase the wear resistance and operational life of some friction pairs in applications where wear can often occur [1-5, 10]. But the hard coatings retain a high coefficient of friction which can generate a large amount of heat. The generated heat greatly increases the operating temperature. The high temperature causes the failure of some important components which render the coatings inappropriate for practical applications.

There are some commonly used soft solid lubricants such as molybdenum disulfide (MoS_2), graphite (C), and boron nitride (BN). MoS_2 is a well-known lamellar solid lubricant with a hexagonal structure [11]. MoS_2 soft coating and its composite soft coating have been widely used for their ultra-low friction. However, the weakness of MoS_2 soft coatings is also very obvious. When the temperature gets to 400℃, MoS_2 soft coating begins to be oxidized to form MoO_3 which can decrease the lubricity of the MoS_2 soft coating sharply [12]. And MoS_2 soft coating is very sensitive to environmental humidity. When the environmental humidity changes from 10% to 90%, the friction coefficient of the MoS_2 soft coating doubles. Therefore, it is necessary to study a new kind of soft coating.

Tungsten disulfide (WS_2) is a novel excellent lamellar solid lubricant. It has physical (prevents adhesion), chemical (high oxidation resistance) and microstructural (lamellar structure with ultra-low shear strength) influence on a tribological contact of working surfaces. The mechanism behind their effective lubricating performance is attributed to easy shearing along the basal planes of the hexagonal crystalline structures named □ texture [13, 14]. Recently, WS_2 coatings have attracted increasing interests for various applications, because of their low friction coefficient [15]. It is thought that these new composite coatings which combine WS_2 coating with other materials have ideal properties for a wide range of applications. It has been proved possible to deposit these composite coatings while retaining their very low friction characteristics, high coating/substrate critical load and high wear resistance in either vacuum or humid air [16, 17]. Deepthi et al. [18] reported that nanocomposite coatings of CrN-WS_2 were prepared at different Cr contents (approximately 8-39 at%) using an unbalanced magnetron sputtering system. And they found that CrN-WS_2 coatings not only exhibited improved adhesive properties and low friction coefficient, but also showed better wear resistance and high hardness.

In the present study, WS_2 coatings (WS_2 and WS_2/Zr) were deposited on the surface of YT15 (WC+15%TiC+6%Co) cemented carbide by medium-frequency magnetron sputtering, multi-arc ion plating and ion beam assisted deposition technique. Microstructural and fundamental properties of these coatings were examined. Sliding wear tests of these coated specimens against 40Cr hardened steel were carried out using a ball-on-disk method in dry friction conditions, and the friction and wear behaviors were investigated.

2 Materials and experimental procedures

2.1 Preparation of PVD WS_2 based coatings

The substrate material employed for this study was YT15 (WC+15%TiC+6%Co) cemented carbide. The physical and mechanical properties of the YT15 cemented carbide are listed in Table 1. The surface of the substrate was mirror-polished and cleaned ultrasonically in ethanol and acetone for 15 min, respectively, and then dried for about 20 min in a pre-vacuum dryer. A multiple use ion planting equipment was employed to deposit the WS_2 coatings. To get the WS_2 coatings, two WS_2 targets

(medium-frequency magnetron sputtering) and one Zr target (multi-arc ion plating) were used. Prior to the deposition, the coating chamber was heated up to 200℃ and the vacuum in the chamber was pumped to 1.0×10^{-3} Pa. Then the substrate was cleaned by argon ion bombardment for 20 min with a bias voltage of -800 V. The WS_2 coating with Zr is named WS-1. For the purpose of comparison, the WS_2 coating without Zr is also deposited on the YT15 cemented carbide, and it is named WS-2. All the coating conditions are listed in Table 2.

Table 1 Properties of the YT15 cemented carbide

Composition (wt.%)	Flexural strength (MPa)	Hardness (GPa)	Density (g/cm^3)	Young's modulus (GPa)	Thermal expansion coefficient (10^{-6}/k)	Poisson's ratio
WC+15%TiC +6%Co	1150	15.5	11.5	510	6.51	0.25

Table 2 Physical vapour deposition coating conditions

Substrate	Deposition temperature (□)	Ar pressure (Pa)	Substrate bias voltage (V)	WS_2 current (A)	Zr current (A)	Deposition time (min)
YT15	200	0.5	-100	1.2	80	150

2.2 Measurement of microstructures and properties of WS_2 coatings

Surface morphologies of the WS_2 coatings were investigated by scanning electron microscopy. The crystallization of □ texture of the WS_2 coating was studied by X-ray diffraction. The coating/substrate critical load of the WS_2 coating was tested on the MFT-4000 device (Multi-functional Tester for Material Surface Properties) by moving the diamond stylus with a 200-μm radius along the examined coating's surface. The scratch parameters for testing the critical load are applied load 80 N, load increase rate 80 N/min, and scratch travel 4 mm. The coating hardness was tested on the MH-6 hardness tester at 0.2-N loads. Prior to the deposition, small adhesive tapes about several millimeters in length and width were marked on the edge of the cemented carbide YT15 disks. The thickness of the WS_2 coating according to the marked adhesive tapes was measured by using the Wyko NT9300 Optical Profiler and the results were confirmed on the cross-sectional view with scanning electron microscope (SEM).

2.3 Friction and wear tests

Sliding wear tests were conducted using the ball-on-disk method with a high-speed nano-micro tribometer (UMT-2, CETR) at room temperature. The disk specimen was made of PVD WS_2 coated carbides and the dimension of the substrate disk was $\Phi 56 \times 4$ mm. The ball ($\Phi 9.525$ mm) was made of 40Cr hardened steel with a hardness of HRC 55-60. The ball surface was polished to produce a final surface roughness of R_a=0.05 μm. Both the ball and the disk were ultrasonically cleaned in ethanol and acetone progressively. The 40Cr hardened steel ball was fixed, while the WS_2 coated carbides disk rotated at a speed of 40-120 m/min. A normal load of 5-25 N was applied in the tests.

The friction coefficients were obtained directly from the above mentioned tribometer's computer. The wear rate W was defined as

$$W = \frac{V}{PL} \tag{1}$$

where V was the volume loss, P was the applied load, and L was the sliding distance. The W was the unit of volume loss per unit force and per unit distance (mm^3/Nm). The worn regions of the coated disk were examined by scanning electron microscopy (SEM) and Wyko NT9300 Optical Profiler.

3 Results and discussion

3.1 Microstructures and properties of WS_2 coatings

The hardness, thickness, and critical load between the coating and substrate of the WS_2 coatings are presented in Table 3. It is revealed that the uncoated YT15 cemented carbide has a hardness of 15.5 GPa (see Table 1). Deposition of the WS_2 or WS_2/Zr coating onto the specimens causes the decrease in surface layer hardness. The hardness of WS-1 (with WS_2/Zr composite coating) is 6.2 GPa, which is just 40% of the substrate's hardness; while the hardness of WS-2 (only with WS_2 coating) shows much more decrease (only 3.5 GPa) compared with that of YT15 and WS-1. The coating thickness of WS-1 (with WS_2/Zr composite coating) is 1.5 μm; while the coating thickness of WS-2 (only with WS_2 coating) shows a little thinner (only 1.2 μm) compared with that of WS-1 (see Table 3).

The critical load characterizing the adherence of the coating to the substrate is determined as the one corresponding to the acoustic emission increase signaling the beginning of spalling of the coating

in scratch test. It is found that the critical load of WS-2 (with WS_2 coating) is 31.61 N; while the critical load of WS-1 (with WS_2/Zr composite coating) shows an increase (43.25 N) compared with the one without Zr (see Table 3). Because the Ⅱ crystal structure of WS_2 is hexagonal layered structure, the shear strength of the WS_2 coating is ultralow. Therefore, the WS_2 coating/substrate critical load is quite low. However, the coating/substrate critical load of the WS_2 coating shows an increase of 37% through adding Zr.

Table 3 Properties of the WS_2 coatings

Specimen	Substrate	Coating	Hardness (GPa)	Thickness (μm)	Critical load (N)
YT15	YT15	-	15.5	-	-
WS-1	YT15	WS_2/Zr	6.2	1.5	43.25
WS-2	YT15	WS_2	3.5	1.2	31.61

Figure 1 shows the surface and cross-sectional SEM micrographs of the WS_2/Zr composite coating. The coating thickness is about 1.5 μm in Fig. 1b. The crystallization of WS_2 coatings were studied by X-ray diffraction (XRD). As a good solid lubricant, the crystal structure of WS_2 is hexagonal layered structure. And the □ texture of WS_2 crystal structure plays an important role in the lubricity of WS_2 coatings. The greater the strength of □ texture of WS_2 crystal structure is, the better the lubricity of WS_2 soft coatings would be. Fig. 2 shows the XRD of WS_2 coatings. There is a diffraction peak of WS_2 at 2θ of 10°~12° which is WS_2 (002) crystal face of □ texture. And it is clear that the WS_2/Zr composite coating has better crystallization than pure WS_2 coating. We can infer that adding Zr can effectively promote the growth of □ texture of the WS_2 coating. The elemental composition of the WS_2 coatings is given in Table 4. It can be obviously seen from Table 4 that both S/W ratios of the WS_2 coatings are less than the S/W proportion of WS_2 compounds. It may be because that the sputtering efficiency of S and W are different, and S may react with other residual gases in the deposition temperature of 200□. Meanwhile, the S/W ratio of WS-1 is 1.724 while that of WS-2 is 1.411 which can prove that adding Zr can effectively promote the growth of WS_2 crystals.

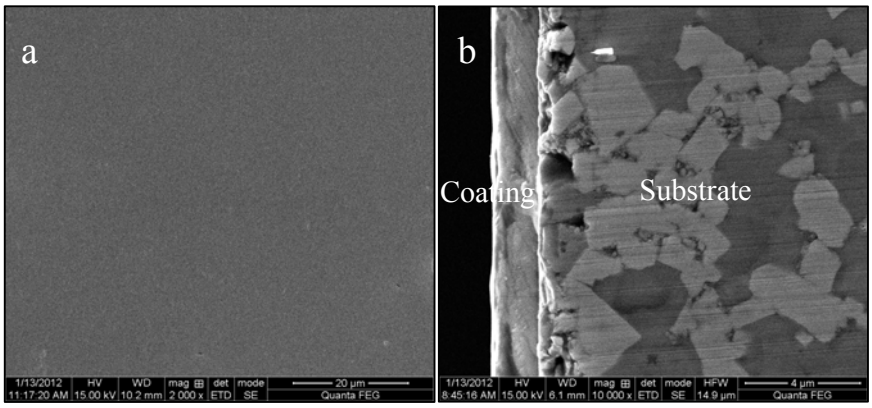

Fig. 1 Surface **a** and cross-section **b** morphologies of WS_2/Zr composite coating

Table 4 Elemental composition of the WS_2 coatings

Specimen	Coating	S (at.%)	W (at.%)	Zr (at.%)	S/W
WS-1	WS_2/Zr	55.45	32.17	12.38	1.724
WS-2	WS_2	58.52	41.48	-	1.411

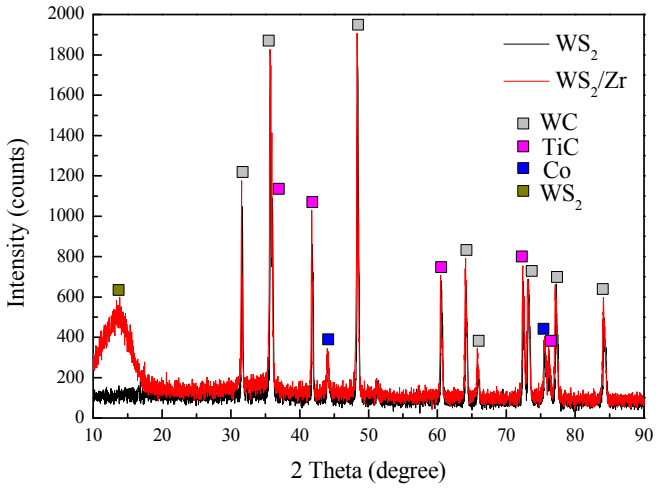

Fig. 2 XRD of WS_2 coatings

3.2 Friction coefficient and wear rates of WS_2 coatings against 40Cr hardened steel

In sliding wear tests, the friction coefficient of WS-1, WS-2 and YT15 cemented carbide was a function of sliding time, and is shown in Fig. 3. As can be seen, the YT15 specimen without coating exhibited the highest friction coefficient; while the WS-1 specimen with WS_2/Zr coating showed the smallest friction coefficient under the same testing conditions. It is obvious that the friction process of YT15 cemented carbide against 40Cr is not smooth, and the friction coefficient fluctuates

significantly especially in the last 150 s. The average friction coefficient of YT15 cemented carbide is about 0.43 in the last 150 s sliding test. The friction coefficient of WS-2 (with WS_2 coating) also shows some fluctuations and the average value is about 0.06 in the first 100 s sliding operation, and then increases to 0.12 in the end. The friction coefficient of WS-1 (with WS_2/Zr coating) fluctuates little and decreases gradually from 0.05 to 0.03 in the first 125 s sliding operation, and then increases gradually from 0.03 to 0.05 in the last 125 s sliding operation.

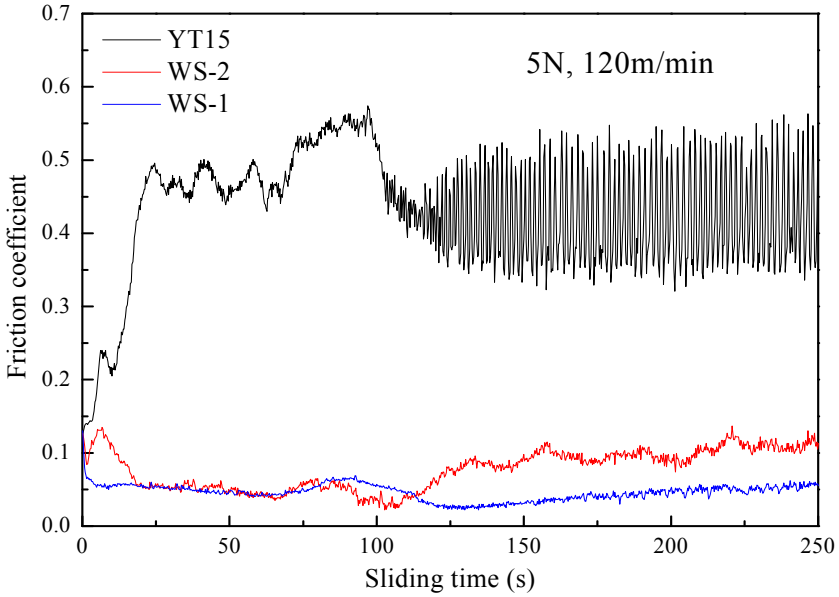

Fig. 3 Variation of friction coefficient with sliding time of YT15, WS-2 and WS-1 specimens when sliding against 40Cr hardened steel balls at a sliding speed of 120 m/min and a load of 5 N

In the sliding wear tests, the average friction coefficient of WS_2 coatings and YT15 cemented carbide against 40Cr hardened steel is a function of applied load and sliding speed, as shown in Figs. 4 and 5 respectively. As can be seen, the WS-1 specimen shows the smallest friction coefficient among all the specimens tested under the same conditions. The friction coefficient increases with the increase of the load while decreases with the increase of sliding speed. The friction coefficient of WS-1 is quite insensitive to the sliding speed (Fig. 5). It does not vary much at sliding speeds ranging from 40 to 120 m/min.

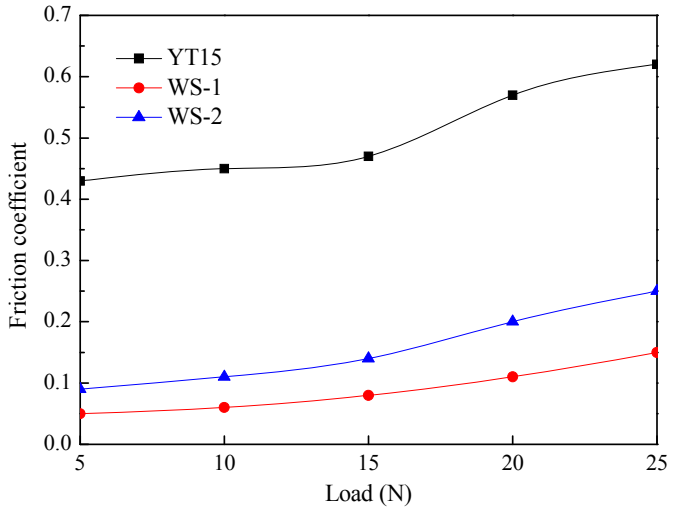

Fig. 4 Friction coefficient of WS_2 coatings and YT15 carbide under different applied loads in sliding wear tests (Sliding speed 120m/min, sliding test time 5 min)

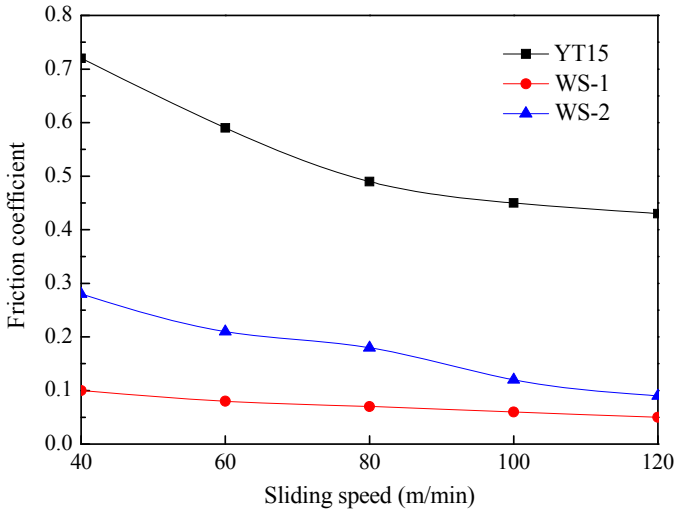

Fig. 5 Friction coefficient of WS_2 coatings and YT15 carbide under different sliding speeds in sliding wear tests (Applied load 5 N, sliding test time 5 min)

Micrographs of the worn surface of the 40Cr hardened steel balls after sliding with three specimens are shown in Fig. 6. Violent wear by plastic ratcheting can be observed on the worn regions of the balls for all specimens. The wear scar diameters of the balls sliding with the YT15, WS-1 and WS-2 specimens are 859.6 μm, 474.2 μm and 602.8 μm, respectively. Obviously, the wear scar diameters of the balls sliding with the WS_2 coatings are much smaller than that of the ball sliding with the YT15 specimen. Meanwhile, the wear scar diameter of the ball sliding with the WS-1 specimen is the smallest one among all the specimens tested under the same sliding conditions.

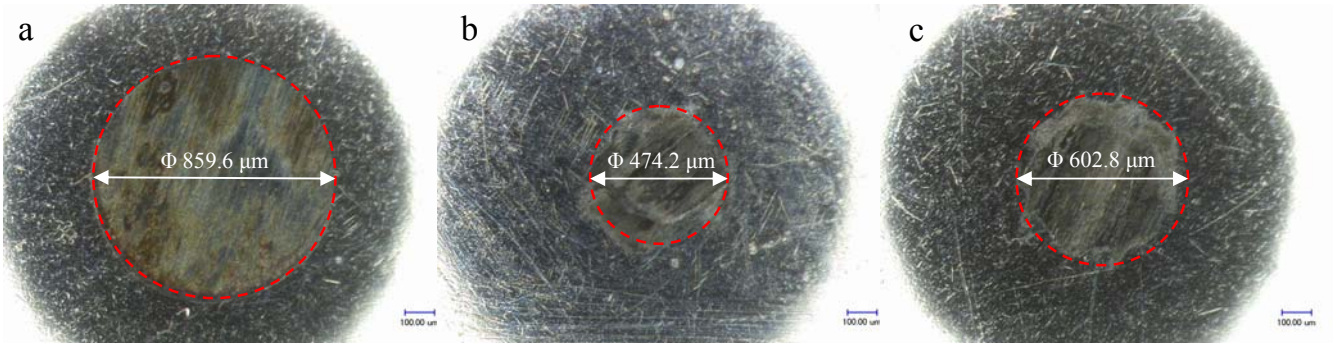

Fig. 6 Micrographs of the worn surface of the 40Cr hardened steel balls after sliding with **a** YT15 specimen, **b** WS-1 specimen, **c** WS-2 specimen (Applied load 5 N, sliding speed 120 m/min, sliding test time 5 min)

The wear segment of the ball can be regarded as a spherical crown [19]. Based on integral operation [20], the wear volume of the worn ball can be calculated as

$$V = \int_{\frac{\sqrt{D^2-d^2}}{2}}^{\frac{D}{2}} \pi\left(\frac{D^2}{4} - y^2\right)dy = \frac{1}{12}\pi D^3 - \frac{1}{24}\sqrt{D^2-d^2}\left(2\pi D^2 + \pi d^2\right) \quad (2)$$

where D is the diameter of the 40Cr hardened steel ball and d is the diameter of the worn scar.

The wear rates of the worn balls sliding with the three specimens can be calculated according to Eqs. (1) and (2). Figs. 7 and 8 show the wear rates of these specimens sliding against 40Cr hardened steel balls as a function of applied load and sliding speed, respectively. It is obvious that the wear rates of WS_2 coating specimens are much lower than that of YT15 specimen and the WS-1 specimen shows the smallest wear rate among all the specimens tested under the same sliding conditions. Meanwhile, the wear rate of WS-1 specimen fluctuates little and almost keeps as a constant value under different applied loads and sliding speeds.

The results confirm that WS_2 coating can greatly improve the tribological behaviour and wear resistance of YT15 carbide. Of the two coated specimens, the WS-2 specimen exhibits significantly lower friction coefficient and wear rates when compared with the YT15 specimen, and the specimen with WS_2/Zr composite coating exhibits further improved friction behaviour and wear resistance under the same test conditions.

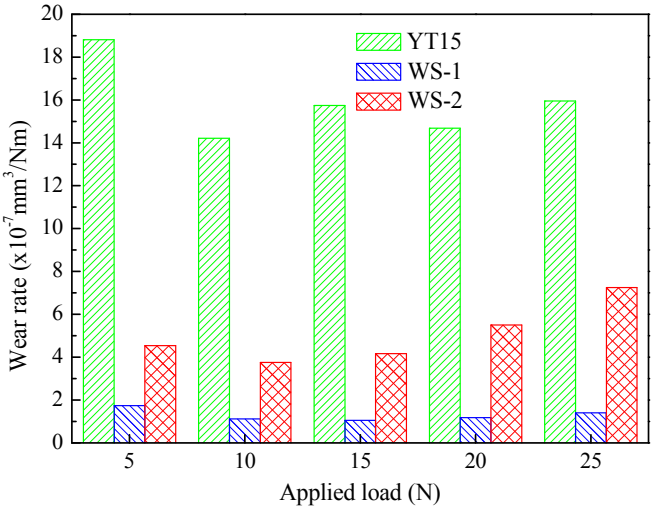

Fig. 7 Wear rates of WS_2 coatings and YT15 carbide under different applied loads in sliding wear test (Sliding speed 120 m/min, sliding test time 5 min)

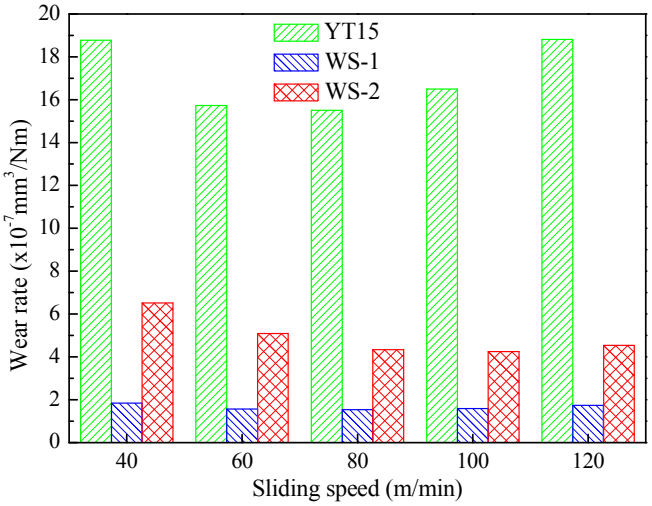

Fig. 8 Wear rates of WS_2 coatings and YT15 carbide under different sliding speeds in sliding wear test (Applied load 5 N, sliding test time 5 min)

3.3 Wear surface studies

The SEM micrograph of the worn surface of WS-2 specimen under a load of 5 N at a sliding speed of 60 m/min after 5 min sliding operation is shown in Fig. 9a. A high magnification examination of the wear track (Fig. 9b) shows that there are some cracks, flakes and delamination on the wear surface. The energy dispersive X-ray spectroscopy (EDX) surface chemical composition analysis on the wear track (point 1 and 2) are illustrated in Fig. 9c and Fig. 9d, respectively. S, W, Fe and O elements are identified at point 1, while C, W and Ti elements are identified at point 2. It is obvious that large areas

of the WS_2 coating on the wear track were worn out, which caused the substrate materials to be exposed during the sliding test.

The SEM micrograph of the worn surface of WS-1 specimen under a load of 5 N at a sliding speed of 60 m/min after 5 min sliding operation is shown in Fig. 10a. It is noted that the wear track width of WS-1 specimen is much smaller than that of WS-2 specimen (see Fig. 9a and Fig. 10a). A high magnification examination of the wear track (Fig. 10b) shows that there are some small mechanical plowing grooves on the wear surface. The energy dispersive X-ray spectroscopy (EDX) surface chemical composition analysis on the wear track (point 1) is illustrated in Fig. 10c. Zr, S, W, Ti, Fe and O elements are identified at point 1. It is clear that the WS-1 specimen exhibited better wear resistance than the WS-2 specimen under the same test conditions. Therefore, adding Zr into WS_2 coating can prolong the antiwear lifetime of WS_2 coating.

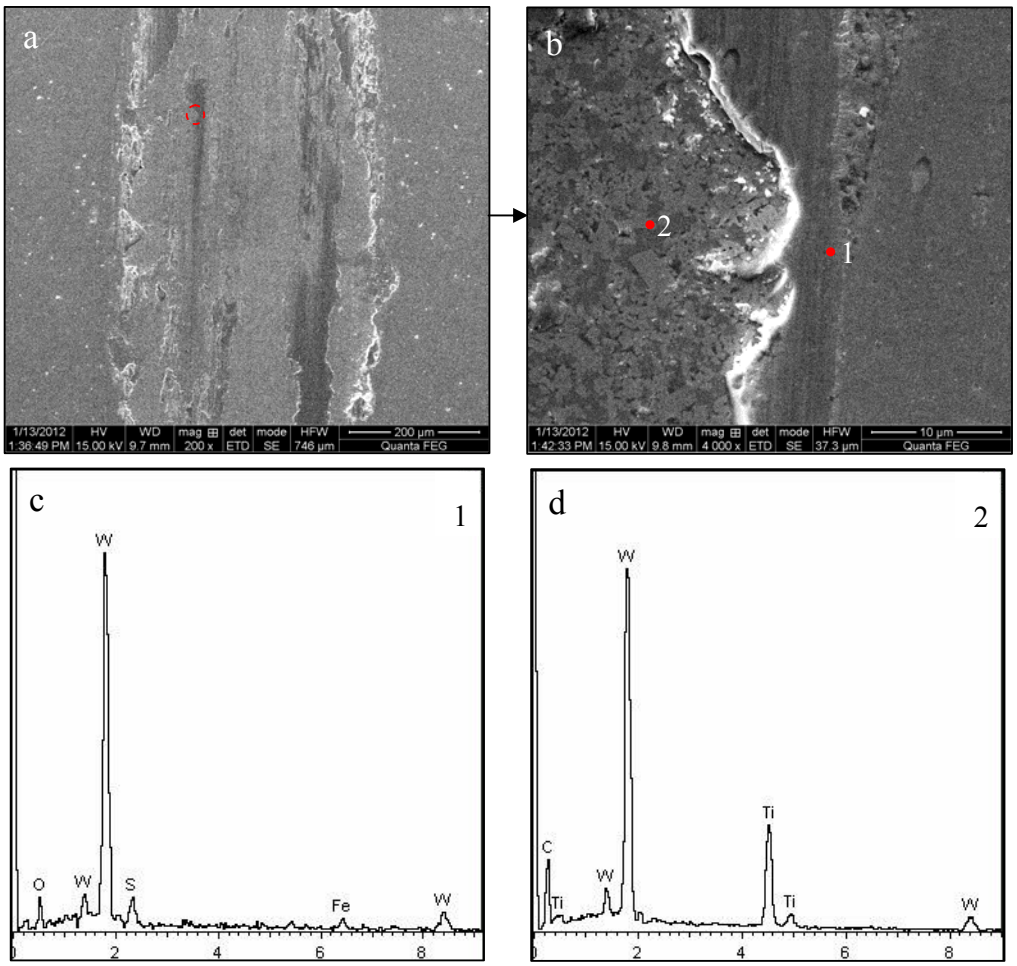

Fig. 9 **a** SEM micrograph of the worn surface of the WS-2 specimen. **b** Enlarged SEM micrograph corresponding to **a**. **c** EDX surface chemical composition at point 1. **d** EDX surface chemical composition at point 2 (Applied load 5 N, sliding speed 60 m/min, sliding test time 5 min)

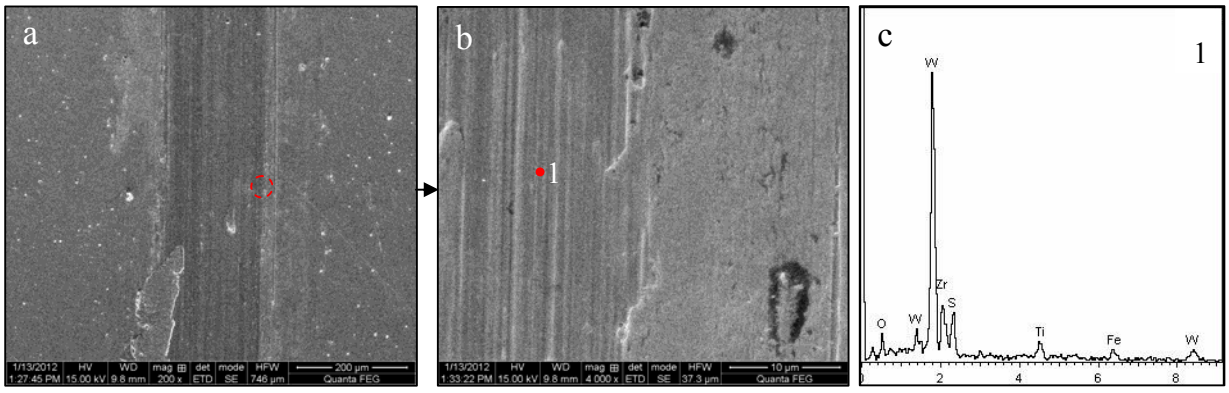

Fig. 10 **a** SEM micrograph of the worn surface of the WS-1 specimen. **b** Enlarged SEM micrograph corresponding to **a**. **c** EDX surface chemical composition at point 1 (Applied load 5 N, sliding speed 60 m/min, sliding test time 5 min)

Fig. 11a shows the SEM micrograph of the wear surface of 40Cr hardened steel ball sliding against WS-1 specimen under a load of 10 N at a sliding speed of 120 m/min after 5 min sliding test. It is noted that the surface of 40Cr hardened steel ball is covered by some materials almost over the whole wear scar. Fig. 11b shows the enlarged SEM micrograph of the adhered material on the wear scar of the 40Cr hardened steel ball corresponding to Fig. 11a. The energy dispersive X-ray spectroscopy (EDX) surface chemical composition analysis on the wear track (point 1 and 2) are illustrated in Fig. 11c and Fig. 11d, respectively. Fe, C and Si elements are identified at point 1, while Zr, S, W, Fe, C, Cr and O elements are identified at point 2. The self-lubricating and wear mechanism of WS_2/Zr coating indicates that WS_2/Zr composite coating was transferred to the surface of 40Cr hardened steel ball and formed a transfer film in the sliding test. Then the friction occurred between the transfer film and the WS_2/Zr composite lubricating film instead of between the cemented carbide YT15 substrate and the 40Cr hardened steel ball. Because of the low shear strength of WS_2/Zr coating, it has ultralow friction coefficient when sliding against 40Cr hardened steel balls. Therefore, friction occurs inside the solid lubricating film which can decrease friction and wear, lower friction coefficient and prolong the lifetime of the friction pairs.

Fig. 12a shows the SEM micrograph of the wear surface of 40Cr hardened steel ball sliding against WS-2 specimen under a load of 10 N at a sliding speed of 120 m/min after 5 min sliding test. It is noted that the wear scar on the surface of the 40Cr hardened steel ball is very obvious and some part of the worn surface is covered with some materials, believed to be WS_2. The energy dispersive X-ray spectroscopy (EDX) surface chemical composition analysis on the wear track (point 1 and 2) are illustrated in Figs. 12b and 12c, respectively. Fe, C, Cr and O elements are identified at point 1, while W, S, Fe, C and Cr elements are identified at point 2. From Fig. 12 we can see that the WS_2 transfer layer is formed but also is severely damaged during the sliding test. The worn surface of the 40Cr hardened steel ball sliding against WS-2 specimen is worse than that against the WS-1 specimen.

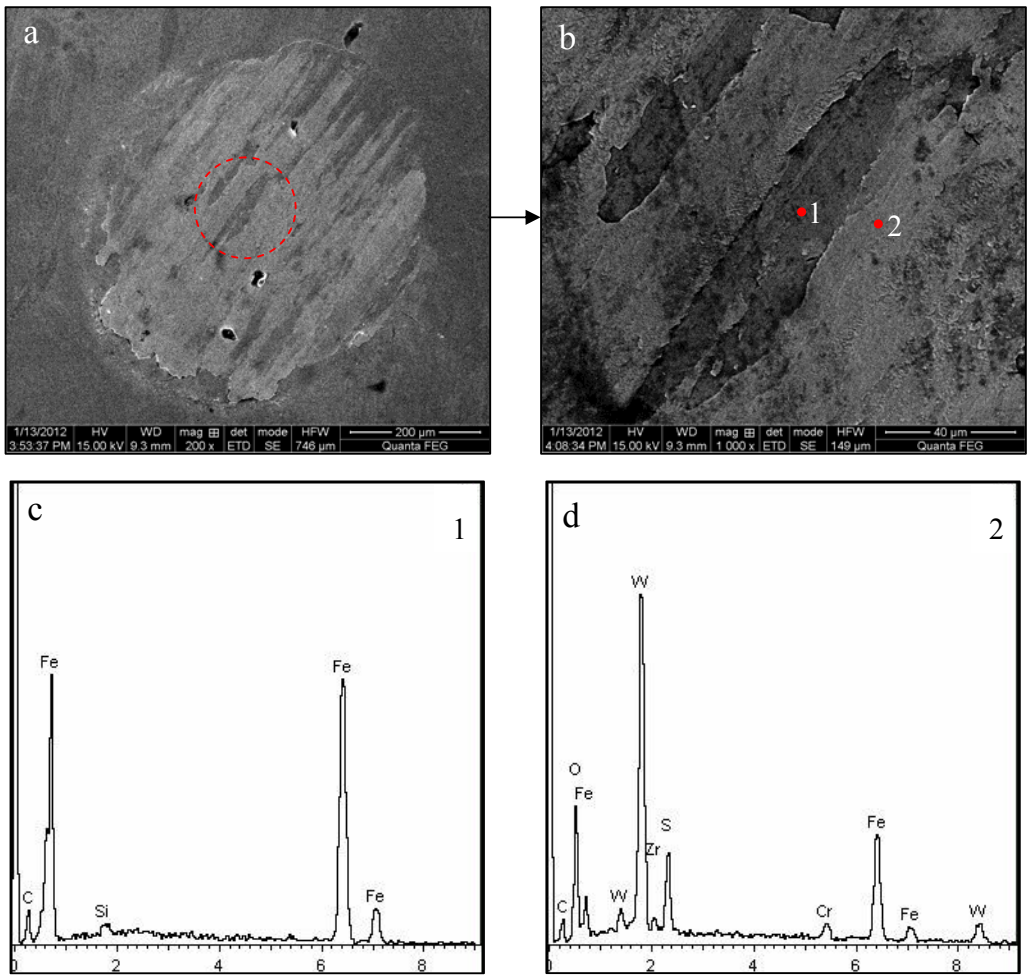

Fig. 11 **a** SEM micrograph of the worn surface of the 40Cr hardened steel ball sliding against WS-1 specimen. **b** Enlarged SEM micrograph corresponding to **a**. **c** EDX surface chemical composition at point 1. **d** EDX surface chemical composition at point 2 (Applied load 10 N, sliding speed 120 m/min, sliding test time 5 min)

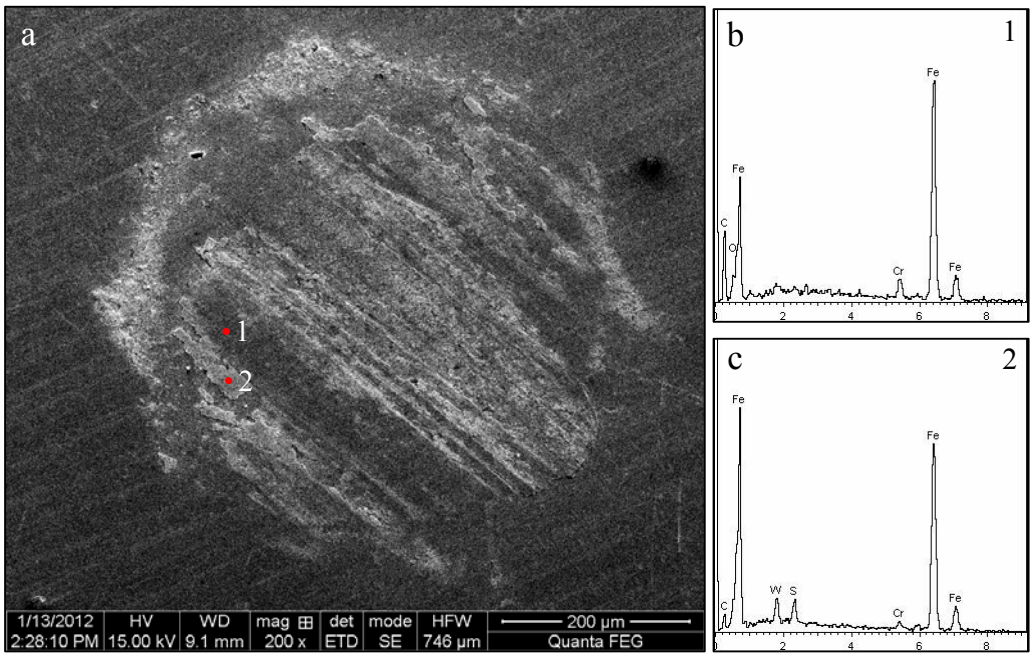

Fig. 12 **a** SEM micrograph of the worn surface of the 40Cr hardened steel ball sliding against WS-2 specimen. **b** EDX surface chemical composition at point 1. **c** EDX surface chemical composition at point 2 (Applied load 10 N, sliding speed 120 m/min, sliding test time 5 min)

4 Conclusions

WS_2 coatings (WS_2 and WS_2/Zr) were deposited by medium-frequency magnetron sputtering, multi-arc ion plating and ion beam assisted deposition technique on the cemented carbide YT15 substrates. Sliding wear tests against 40Cr hardened steel using a ball-on-disk tribometer method were carried out with these coated materials. The main conclusions obtained can be summarized as follows.

1. The WS-1 specimen (with WS_2/Zr composite coating) has the higher hardness and coating/substrate critical load compared with that of the WS-2 specimen (only with WS_2 coating).
2. The WS-1 specimen shows the smallest friction coefficient among all the specimens tested under the same conditions. The friction coefficient of WS-1 specimen increases with the increase in applied load, and is quite insensitive to the sliding speed.
3. The WS-1 specimen shows the smallest wear rate among all the specimens tested under the same conditions and it almost remains constant under different applied loads and sliding speeds.

The WS-1 specimen exhibits improved friction behavior and wear resistance compared to that of the WS-2 specimen. The antiwear lifetime of the WS_2 coatings can be prolonged through adding Zr additives.

4. The self-lubricating and wear mechanism of WS_2/Zr coating indicates that WS_2/Zr composite coating is transferred to the surface of 40Cr hardened steel ball and forms a transfer film in the sliding test. Then the friction occurs between the transfer film and the WS_2/Zr composite lubricating film instead of between cemented carbide YT15 substrate and 40Cr hardened steel ball. Because of the low shear strength of WS_2/Zr coating, it has ultralow friction coefficient when sliding against 40Cr hardened steel balls. Therefore, friction occurs inside the solid lubricating film which can decrease friction and wear, lower friction coefficient and prolong the lifetime of the friction pairs.

Acknowledgments This work is supported by "National Natural Science Foundation of China (51375271)", "Taishan Scholar Program of Shandong Province", "Independent Innovation Foundation of Shandong University (2011JC001)" and "Specialized Research Fund for Doctoral Program of Higher Education (20110131130002)".

References

[1] Klocke, F., Krieg, T.: Coated tools for metal cutting – features and applications. CIRP Ann. – Manu. Tech. **48**, 515-525 (1999)

[2] Prengel, H.G., Pfouts, W.R., Santhanam, A.T.: State of the art in hard coatings for carbide cutting tools. Surf. and Coat. Tech. **102**, 183-190 (1998)

[3] Kalss, W., Reiter, A., Derflinger, V., Gey, C., Endrino, J.L.: Modern coatings in high performance cutting applications. Int. J. of Refra. Met. and Hard Mater. **24**, 399-404 (2006)

[4] Renevier, N.M., Fox, V.C., Teer, D.G., Hampshire, J.: Coating characteristics and tribological properties of sputter-deposited MoS_2/metal composite coatings deposited by closed field unbalanced magnetron sputter ion plating. Surf. and Coat. Tech. **127**, 24-37 (2000)

[5] Ezugwu, E.O., Okeke, C.I.: Tool life and wear mechanisms of TiN coated tools in an intermittent cutting operation. J. of Mater. Proce. Tech. **116**, 10-15 (2001)

[6] Fenske, G.R.: Nitride and carbide coatings for high speed steel cutting tools. Tribol. Tran. **32**, 339-345 (1989)

[7] Sahin, Y., Sur, G.: The effect of Al_2O_3, TiN and Ti (C, N) based CVD coatings on tool wear in machining metal matrix composites. Surf. and Coat. Tech. **179**, 349-355 (2004)

[8] Jindal, P.C., Santhanam, A.T., Schleinkofer, U., Shuster, A.F.: Performance of PVD TiN, TiCN, and TiAlN coated cemented carbide tools in turning. Int. J. of Refra. Met. and Hard Mater. **17**, 163-170 (1999)

[9] Harris, S.G., Doyle, E.D., Vlasveld, A.C., Audy, J., Long, J.M., Quick, D.: Influence of chromium content on the dry machining performance of cathodic arc evaporated TiAlN coatings. Wear **254**, 185-194 (2003)

[10] Deng, J.X., Liu, J.H., Zhao, J.L., Song, W.L., Niu, M.: Friction and wear behaviors of the PVD ZrN coated carbide in sliding wear tests and in machining processes. Wear **264**, 298-307 (2008)

[11] Martins, R.C., Paulo, S.M., Seabra, J.O.: MoS_2/Ti low-friction coating for gears. Tribol. Int. **39**, 1686-1697 (2006)

[12] Song, W.L., Deng, J.X., Zhang, H., Yan, P.: Study on cutting forces and experiment of MoS_2/Zr-coated cemented carbide tool. Int. J. of Adv. Manu. Tech. **49**, 903-909 (2010)

[13] Sadale, S.B., Patil, P.S.: Synthesis and characterization of type-□ textured tungsten disulfide thin films by vdWR process with Pb interfacial layer as texture promoter. J. of Crystal Growth **290**, 363-368 (2006)

[14] Lian, Y.S., Deng, J.X., Li, S.P.: Influence of the deposition temperature on the properties of medium-frequency magnetron sputtering WS_2 soft coated tools. Adv. Mater. Res. **472-475**, 44-49 (2012)

[15] Zhu, L.N., Wang, C.B., Wang, H.D., Xu, B.S., Zhuang, D.M., Liu, J.J., Li, G.L.: Tribological properties of WS_2 composite film prepared by a two-step method. Vacuum **85**, 16-21 (2010)

[16] Du, G.Y., Ba, D.C., Wang, X.G.: Effects of Ti/Ni transition layers on frictional behavior of tungsten disulfide thin film. Tribology **29**, 146-151 (2009)

[17] Zheng, X.H., Tu, J.P., Lai, D.M., Peng, S.M., Gu, B., Hu, S.B.: Microstructure and tribological behavior of WS_2-Ag composite films deposited by RF magnetron sputtering. Thin Solid Films **516**, 5404-5408 (2008)

[18] Deepthi, B., Barshilia, H.C., Rajam, K.S., Konchady, M.S., Pai, D.M., Sankar, J.: Structural, mechanical and tribological investigations of sputter deposited CrN-WS_2 nanocomposite solid lubricant coatings. Tribol. Int. **44**, 1844-1851 (2011)

[19] Ma, W.L., Lu, J.J.: Effect of surface texture on transfer layer formation and tribological behavior of copper-graphite composite. Wear **270**, 218-229 (2011)

[20] He, C.X.: Advanced Mathematics. Tsinghua University Press, Beijing (2009)